Convergence of undulatory swimming kinematics across a diversity of fishes

Valentina Di Santo[a,b,1,2], Elsa Goerig[a,c,1,2], Dylan K. Wainwright[a,d], Otar Akanyeti[e,f], James C. Liao[f], Theodore Castro-Santos[c], and George V. Lauder[a]

[a]Museum of Comparative Zoology, Harvard University, Cambridge, MA 02138; [b]Division of Functional Morphology, Department of Zoology, Stockholm University 114 19 Stockholm, Sweden; [c]U.S. Geological Survey-Eastern Ecological Science Center, S.O. Conte Research Laboratory, Turners Falls, MA 01376; [d]Department of Ecology and Evolutionary Biology, Yale University, New Haven, CT 06520; [e]Department of Computer Science, Aberystwyth University, Aberystwyth SY23 3FL, United Kingdom; and [f]Department of Biology, The Whitney Laboratory for Marine Bioscience, University of Florida, St. Augustine, FL 32080

Edited by David Jablonski, The University of Chicago, Chicago, IL, and approved November 1, 2021 (received for review July 23, 2021)

Fishes exhibit an astounding diversity of locomotor behaviors from classic swimming with their body and fins to jumping, flying, walking, and burrowing. Fishes that use their body and caudal fin (BCF) during undulatory swimming have been traditionally divided into modes based on the length of the propulsive body wave and the ratio of head:tail oscillation amplitude: anguilliform, subcarangiform, carangiform, and thunniform. This classification was first proposed based on key morphological traits, such as body stiffness and elongation, to group fishes based on their expected swimming mechanics. Here, we present a comparative study of 44 diverse species quantifying the kinematics and morphology of BCF-swimming fishes. Our results reveal that most species we studied share similar oscillation amplitude during steady locomotion that can be modeled using a second-degree order polynomial. The length of the propulsive body wave was shorter for species classified as anguilliform and longer for those classified as thunniform, although substantial variability existed both within and among species. Moreover, there was no decrease in head:tail amplitude from the anguilliform to thunniform mode of locomotion as we expected from the traditional classification. While the expected swimming modes correlated with morphological traits, they did not accurately represent the kinematics of BCF locomotion. These results indicate that even fish species differing as substantially in morphology as tuna and eel exhibit statistically similar two-dimensional midline kinematics and point toward unifying locomotor hydrodynamic mechanisms that can serve as the basis for understanding aquatic locomotion and controlling biomimetic aquatic robots.

fish locomotion | biomechanics | BCF | swimming modes | undulatory swimming

During steady aquatic locomotion, animals exert force against the surrounding water to support and move their body (1, 2). Energy transfer from body to medium is achieved through reaction forces (e.g., viscous, form, and induced drag), which are all contingent on the shape, size, and motion of the body and propulsors (e.g., fins, in the case of fishes) (3–8). Many fish species primarily use their body and caudal fin (BCF) for undulatory propulsion and are grouped into four major modes depending on head amplitude and the length of the propulsive wave during body undulation (8, 9). These modes are classically characterized by an expected decreasing gradient in head:tail oscillation during undulation from anguilliform ("eel-like") locomotion, supposedly showing the largest relative side-to-side amplitude of the head (yaw), to thunniform ("tuna-like") locomotion, showing the least amount of yaw, with two intermediate modes: subcarangiform ("trout-like") and carangiform ("mackerel-like"). According to this classification, fish species are also expected to undulate different portions of their body at different amplitudes: anguilliform swimmers have an elongated body and are expected to undulate the majority of their body (10); subcarangiform swimmers are expected to move both their trunk and tail; carangiform swimmers may move only the posterior third portion of their body; and, finally, thunniform swimmers may hold most of their body relatively straight and only use their narrow caudal peduncle and tail for forward propulsion (9). Based on this classification, the expectation is to find a decrease in amplitude and an increase in wavelength from anguilliform to thunniform modes. Even though Breder (7) and others (9–12) recognized that these categories represent "average types within an essentially continuous range of swimming modes" and thus should not be applied strictly, fishes have frequently been placed into one of these categories based on general morphological features of body elongation and stiffness (13). In fact, many recent studies continue to work under this framework to investigate an array of fish BCF swimming (13–19). The systematic assignment of fishes into one of these categories becomes problematic when the use of incorrect a priori assumptions about locomotor patterns leads to biased interpretation of correlations between swimming kinematics and ecology. This may limit our ability to understand the diversity of fish locomotion and to correctly program fish-like robotic platforms (18, 20–22) or to

Significance

Swimming ability has contributed to the evolutionary success of fishes, and its mechanics have been studied extensively. Most fishes swim primarily through undulation of their body and caudal fin (BCF) and have been historically divided into four major kinematic modes based on their morphology. Here, we compare kinematics of BCF locomotion in 44 species. Contrary to expectations and despite considerable morphological diversity, fishes share major kinematic features during steady swimming and are placed on a continuum rather than in discrete categories. This suggests a unifying BCF mechanism to generate efficient aquatic propulsion. Our work reevaluates a well-established hypothesis in biomechanics, highlighting the importance of avoiding a priori partitioning of fishes into modes, to further our understanding of aquatic locomotion.

Author contributions: G.V.L. designed research; V.D.S., E.G., D.K.W., O.A., J.C.L., T.C.-S., and G.V.L. performed research; V.D.S., E.G., D.K.W., O.A., T.C.-S., and G.V.L. analyzed data; and V.D.S. and E.G. wrote the paper.

The authors declare no competing interest.

This article is a PNAS Direct Submission.

[1]V.D.S. and E.G. contributed equally to this work.

[2]To whom correspondence may be addressed. Email: valentina.disanto@zoologi.su.se or goerig.elsa@gmail.com.

This article contains supporting information online at http://www.pnas.org/lookup/suppl/doi:10.1073/pnas.2113206118/-/DCSupplemental.

Published December 1, 2021.

integrate fish biomechanics data into ecological studies and conservation programs (19, 21).

Here, we present a quantitative and comparative empirical study of fish swimming kinematics with the fundamental goal of testing the hypothesis that the classically defined fish BCF swimming modes indeed represent distinct kinematic patterns which also correlate with morphological differences in fishes (such as body elongation and depth) along a gradient from anguilliform to thunniform. We analyzed steady swimming kinematics of 44 species (n = 1 to 6 individuals per species) during steady swimming in sustained, prolonged, or sprint modes at four research facilities (*SI Appendix*, Fig. S1). These included jawless fishes (three species), cartilaginous (three species), and bony fishes (37 species) and, in addition, one species of "fish-like" chordate, the Mediterranean amphioxus *Branchiostoma lanceolatum* (Dataset S1). Sequences of complete tail beat cycles were extracted for each individual, and midlines of the fish were digitized throughout the tail beat and divided into 200 points along the body. Kinematic parameters such as amplitude and phase of lateral oscillation along the body, tail-beat frequency, wavelength, and curvature were quantified and expressed as a proportion of body length (BL). External morphological traits including width and depth at various locations along the body as well as the fineness ratio were calculated on museum specimens (n = 1 to 3) for each of the tested species. Our study shows that, in contrast to the widespread assumption that BCF locomotion can be divided into discrete modes, many fish species are located on a continuum and exhibit a generally statistically similar suite of undulatory kinematic parameters during steady locomotion, with oscillation amplitude accurately described using a unifying second-order polynomial equation. Therefore, we conclude that the classical fish swimming modes are poor descriptors of the diversity of fish BCF locomotor kinematics.

Results

We analyzed 151 video sequences across all the species used in this study. Seven species (16%) had a sample size of one individual, while 33 (75%) had sample sizes between two and six. We analyzed 10 sequences for each of the four canonical species traditionally used to define fish BCF swimming modes (American eel *Anguilla rostrata*, brook trout *Salvelinus fontinalis*, mackerel *Scomber scombrus*, and tuna *Thunnus albacares*) to identify intraspecific variation in kinematic features (n = 5 for each species swimming at about 1 BL × s^{-1}). Reynolds numbers (Re) were > 1,000 (median = 110,288, interquartile range [IQR] = 60,370 to 753,319, except for amphioxus moving in still water [mean Re = 568]). Strouhal numbers (STs) ranged from 0.15 to 0.82, with a median of 0.29 and an IQR of 0.24 to 0.35 (*SI Appendix*, Fig. S2). Swimming speeds varied greatly across testing conditions and apparatus: fish tested in small flow tanks and tunas tested in a large circular tank exhibited swim speeds ranging from 0.2 to 13 BL × s^{-1}, while fish tested in the large outdoor experimental flume had swim speeds ranging from 1 to 25 BL × s^{-1}. Except for a strong correlation with tail-beat frequency (r = 0.95), swim speed had little effect on kinematic parameters, showing no significant correlation with head amplitude (r = 0.08), maximum amplitude (r = 0.18), wavelength (r = −0.03), or curvature (r = 0.02) (*SI Appendix*, Figs. S3 and S4). Therefore, we compared kinematics across all species regardless of swimming speed.

Kinematics of the Four Canonical Species. During steady locomotion, thrust is generated by an axial undulating wave passing down the body of fishes. When we compared steady swimming kinematics of the four representative species at ∼1 BL × s^{-1} (n = 5 each), wavelength was significantly different (one-way ANOVA, F = 7.70, P = 0.0024), with the mean wavelength of the eel being statistically shorter (0.58 BL) than that of the trout, mackerel, or tuna (1.00, 0.96, and 1.17 BL, respectively; Tukey–Kramer multiple comparison test, α = 0.05). Head amplitude was also significantly different (one-way ANOVA, F = 10.56, P = 0.0005), with the mean head amplitude of the tuna greater than that of the eel, trout, or mackerel (Tukey–Kramer multiple comparison test, α = 0.05). We also found an overall difference among the four swimming modes in tail amplitude (one-way ANOVA, F = 3.37, P = 0.047), but none of the post hoc comparisons among modes were statistically different (Tukey–Kramer multiple comparison test, α = 0.05). The ratio of head:tail amplitude was only statistically higher in the tuna (one-way ANOVA, F = 18.64, P < 0.001). Finally, we found that maximum curvature was not statistically different among the four model species (one-way ANOVA, F = 3.16, P = 0.05). A post hoc power analysis indicated that sample size was adequate to detect differences between modes for wavelength (power = 0.96) head and head:tail amplitude (power = 0.99 for both) but not for tail amplitude (power = 0.62) or maximum curvature (power = 0.64).

When analyzing sequences (n = 10 for each species) across all speeds tested, wavelength was statistically different (one-way ANOVA, F = 12.96, P < 0.0001), with the tuna's wavelength significantly longer than those of the mackerel and eel but not significantly different from the trout's (Tukey–Kramer multiple comparison test, α = 0.05, Fig. 1). Head amplitude was also different across species (one-way ANOVA, F = 4.95, P = 0.005), with eels and tunas having the highest head amplitude (Fig. 1). However, we observed no significant difference in tail and head:tail amplitude (one-way ANOVA, F = 2.31, P = 0.09, and F = 2.48, P = 0.07, respectively, Fig. 1). We observed no differences in maximum curvature among the four model species (one-way ANOVA, F = 1.40, P = 0.1). The post hoc power analysis showed that the sample size was adequate to detect differences in head amplitude (power = 0.87) and wavelength (power = 0.99), but there was high variation for the same sample size in maximum curvature, tail amplitude, and head:tail amplitude (power = 0.5 for all three).

Kinematics across All Species. The wavelength decreased significantly from thunniform (median = 1.14) to subcarangiform (median = 0.93) and anguilliform species (median = 0.75) (one-way ANOVA, F = 8.26, P < 0.001, power = 0.99; Fig. 2*A* and *SI Appendix*, Fig. S6). Overall, species classified as anguilliform had more than one wave passing down their body during the tailbeat, while thunniform species had less than one (*SI Appendix*, Fig. S6). However, we observed subcarangiform species such as the Atlantic salmon *Salmo salar* exhibiting shorter wavelengths (0.74 BL) than most other species and amphioxus having long wavelengths of 1.04 to 1.49 BL. Some species (rainbow trout *Oncorhynchus mykiss*, brook trout, yellowfin tuna, crevalle jack *Caranx hippos*, and short-nose sturgeon *Acipenser brevirostrum*) also showed high variability in wavelength, with an SD around 20% of BL.

Overall, amplitude increased nonlinearly from head (median = 0.03, IQR = 0.02 to 0.05) to tail (median = 0.18, IQR = 0.15 to 0.21), with the rate of increase being much lower in the anterior third of the body and a rapid increase posterior to the midbody location (Fig. 2*B* and *SI Appendix*, Fig. S5). Maximum amplitude always occurred at the tail (starting at 90% down the BL). We found high inter- and intraspecific variation in amplitude along the body within each a priori group. Variability was larger for species classified as anguilliform and subcarangiform. When considering all swimming speeds tested, mean head amplitude was highest in anguilliforms and lowest in carangiforms (one-way ANOVA, F = 6.45, P < 0.001, power = 0.96; Fig. 3*B*). The mean tail amplitude was also highest in anguilliforms than in the other

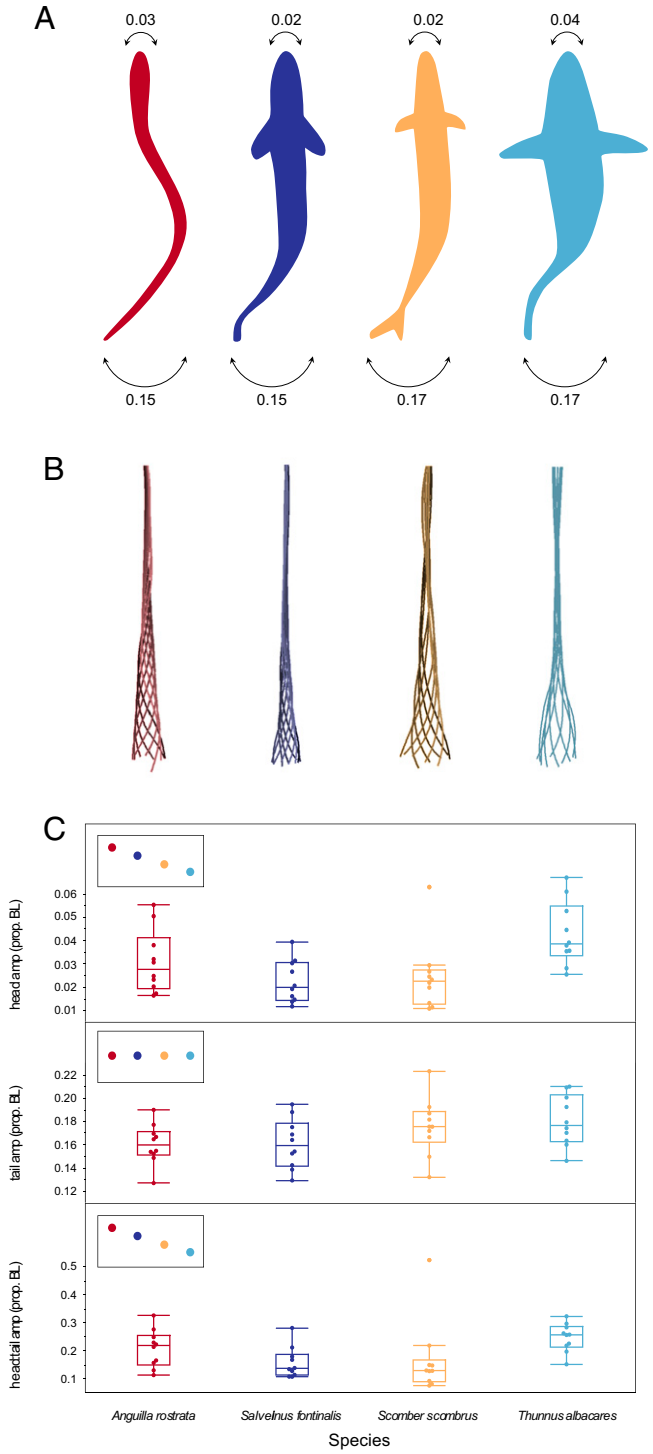

Fig. 1. Rethinking swimming modes in fishes. (*A*) New view based on high-speed video analysis of steady swimming kinematics to illustrate the considerable similarity among the four classic fish swimming modes. Head and tail amplitude variables do not distinguish the four classic categories of BCF swimmers: eel (*Anguilla rostrata*), trout (*Salvelinus fontinalis*), mackerel (*Scomber scombrus*), and tuna (*Thunnus albacares*). (*B*) Representative midlines (average of $n = 10$ each) of complete tail beat cycles of eel, trout, mackerel, and tuna during steady swimming. (*C*) Distribution of head, tail, and head:tail amplitude reported as a proportion of BL in four representative species ($n = 10$ clips per species). The boxes show the median as well as the 25th and 75th, while whiskers show the 10th and 90th. (*Top Left Insets*) Expected pattern based on the canonical classification of swimming modes.

groups (one-way ANOVA, F = 5.63, $P = 0.001$, Tukey–Kramer multiple comparison test, $\alpha = 0.05$, power = 0.94). Some species in the anguilliform group exhibited high values of head:tail amplitude such as amphioxus (0.74) and hagfishes (0.38 and 0.47). As a consequence, species classified a priori as anguilliform had statistically higher head:tail amplitude, especially when compared to carangiform species (one-way ANOVA, F = 3.19, $P = 0.02$, Tukey–Kramer multiple comparison test, $\alpha = 0.05$, power = 0.73). We found that the amplitude envelope of 90% of the tested individuals can be described adequately ($R^2 > 0.9$) using a second-degree polynomial (Fig. 3). An analysis of polynomial coefficients shows that individual datasets are not separated by the swimming modes and instead represent a continuum in the parameter space. We also found that these coefficients covary, suggesting that they are not independent from each other. In particular, there is a strong negative correlation between the linear and quadratic terms ($r = -0.89$, $P < 0.001$). A global model was then fitted using these individual midlines, allowing us to describe 60% of the variability in the amplitude envelope of all studied species with a single equation:

$$y = 0.05 - 0.13x + 0.28x^2.$$

Phase, representing the timing of the undulatory movement along the body, increases linearly from head to tail and shows a similar pattern among species, except for tunas that exhibit lower values posteriorly, which reflects a change in the wave speed at the tail (Fig. 2*C*). Curvature increases gradually as the propulsive wave travels down the body, except for a local minimum at ~20 to 25% of the body length, with a median curvature of 0.88 and an IQR of 0.34 to 2.09 (Fig. 2*D*). Species classified as anguilliform show an increased curvature in the first half of their body by comparison to those classified in the other modes. Maximum values of curvature then always occur posteriorly, beyond the caudal peduncle (median across species = 3.53 BL^{-1}, IQR = 2.22 to 5.12 BL^{-1}). Anguilliform and subcarangiform swimmers, however, exhibited overall higher variability in curvature along their bodies than fish classified in the other modes. Maximum curvature was significantly different across modes (one-way ANOVA, F = 4.46, $P = 0.005$, power = 0.87), with anguilliform and subcarangiform statistically similar to thunniform but not to carangiform (Tukey–Kramer multiple comparison test, $\alpha = 0.05$), which had lower maximum curvature.

We used a multivariate analysis to identify patterns in the multidimensional fish kinematic and morphological space. We selected the first three components from a principal component analysis (PCA), which had eigenvalues equal to or greater than one and accounted for 72% of the variability in the data. The first two components accounted for 62% of the variability (Fig. 4*A*). The first component was mainly composed of morphometric variables, while kinematics contributed primarily to the second component. There was a substantial overlap among swimming modes with regards to kinematics and morphometrics. However, a large proportion of the anguilliform swimmers, characterized by a high fineness ratio, distinctively groups on the morphology axis (Fig. 4*A*). The density-based clustering approach conducted on morphometrics identified one large cluster regrouping 36 species (Fig. 4*B*) sharing similar morphometrics. Seven points, however, remained unassigned: five species closely located in the multivariate space and characterized by a high fineness ratio (>1.5) and low body and peduncle width and depth (amphioxus, American eel, Pacific hagfish *Eptatretus stoutii*, Atlantic hagfish *Myxine glutinosa*, and sea lamprey *Petromyzon marinus*) as well as two species characterized by deeper bodies (Atlantic spadefish *Chaetodipterus faber* and bluegill *Lepomis macrochirus*). When conducted on undulatory kinematics, this approach identified one cluster regrouping all species

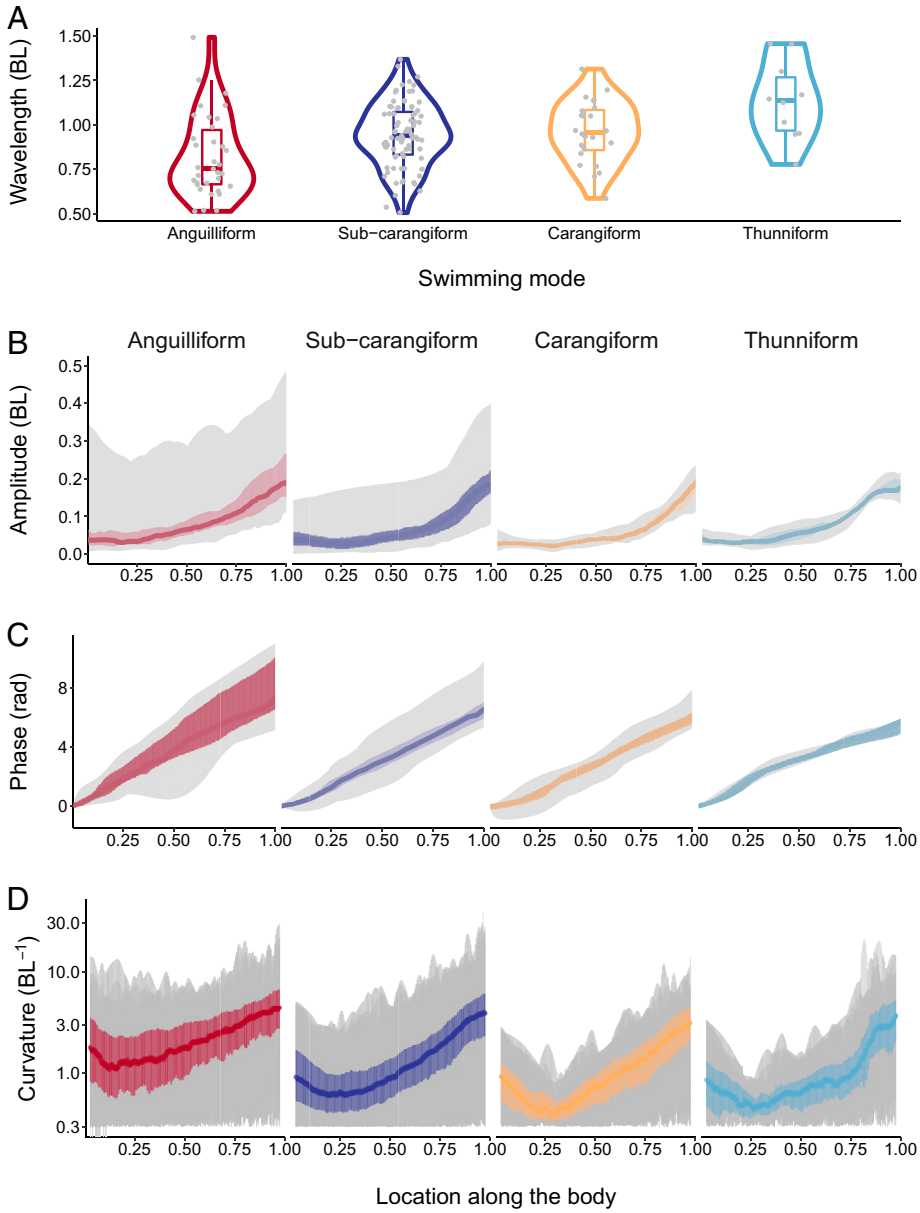

Fig. 2. Two-dimensional kinematics do not support the classical view of fish swimming modes. Representative kinematics (*A*) wavelength, (*B*) amplitude, (*C*) phase, and (*D*) curvature along the body reported as a proportion of BL (*A*, *B*, and *D*) and radians (*C*) across 43 different species of fish and a species of chordate, the Mediterranean amphioxus (*Branchiostoma lanceolatum*). Each data point represents one individual, and species are divided according to the classic swimming modes: "anguilliform," red ($n = 12$), "subcarangiform," dark blue ($n = 27$), "carangiform," orange ($n = 4$), and "thunniform," light blue ($n = 1$). The solid line and colored area represent the median and the IQR, respectively. The gray dots (*A*) and area (*B*–*D*) represent the total variability. The length of the propulsive wave shows high variability within modes but generally increases from eel to tuna with similar values for subcarangiform and carangiform modes. Amplitude increases nonlinearly in a rostro-caudal axis for all tested species with very similar median and IQR values. A specific pattern is visible for tunas in whom the increase in amplitude reaches a plateau near the caudal peduncle. Phase increases linearly from head to tail and is similar among species except for tunas in whom phase values in the posterior body are lower, reflecting a change in the wave speed at the tail. Curvature patterns along the body are similar among swimming modes, reaching maximal values in the anterior part of the tail. Anguilliform swimmers, however, show an overall higher curvature anteriorly (first 2/3 of their body). Variability is greater among the anguilliform and subcarangiform modes for all kinematic parameters; however, this increased variability may partly reflect that these modes represent most of the tested species, while the carangiform and thunniform modes only comprised four and one species, respectively. Thus, the potential for an increased diversity in kinematics patterns is higher for the anguilliform and subcarangiform modes.

except for two unassigned points, the largemouth bass *Micropterus salmoides* and the rainbow trout, both characterized by a large curvature (Fig. 4*C*). This indicates that, despite some differences, there was substantial overlap in the BCF swimming kinematics of the studied species, making it difficult to distinguish groups of species sharing a distinct suite or mode of steady swimming kinematics.

Discussion

Since their first mention by Breder in 1926 (7), the canonical view of BCF modes has been repeated in virtually all reviews of fish locomotion (11, 12, 17), in numerous recent research papers (14–16, 19, 23), and used to categorize fishes based on their presumed kinematic groups. This view has important implications for fisheries conservation and management outcomes because fishing

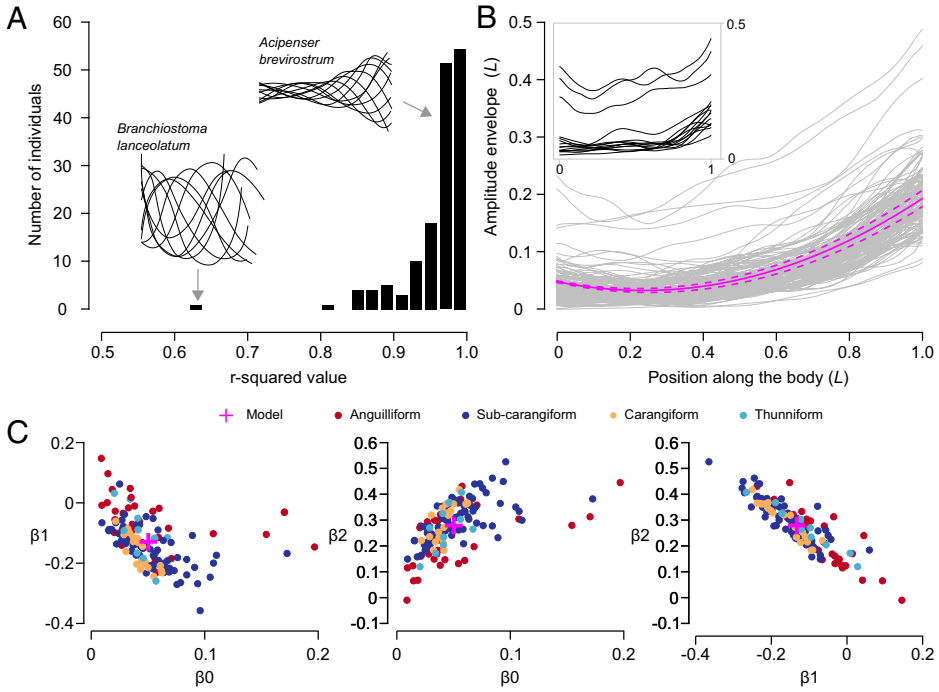

Fig. 3. A representation of fish amplitude envelopes using a second-degree polynomial. (*A*) The frequency distribution of r-squared values for modeled individual amplitude envelopes. The midlines from two representative species are shown as examples: *Acipenser brevirostrum* ($R^2 \geq 0.9$) and *Branchiostoma lanceolatum* ($R^2 \leq 0.7$). (*B*) Fish amplitude envelopes with $R^2 \geq 0.9$ (gray). One representative polynomial model fitted to all fish datasets with 95% CIs (magenta solid and dashed lines) is also shown ($y = 0.05 - 0.13x + 0.28x^2$, r-squared = 0.59, $P < 0.001$). (*Top Left Inset*) Outlier datasets with $R^2 \leq 0.9$. (*C*) Polynomial coefficients; β_0 versus β_1 (*Left*, $r = -0.27$, $P < 0.001$), β_0 versus β_2 (middle, $r = 0.31$, $P < 0.001$), and β_1 versus β_2 (*Right*, $r = -0.89$, $P < 0.001$). Each data point (filled circles) represents one individual, and species are divided according to the classic swimming modes: "anguilliform," red, "subcarangiform," dark blue, "carangiform," orange, and "thunniform," light blue. The global polynomial model from *B* (magenta cross) is also shown.

gear, habitat restoration, and fish passage devices or exclusion barriers are often designed for species placed in different swimming modes (11, 19). Additionally, BCF modes have served as a touchstone for fish-inspired robotic platforms (17, 20, 22, 24). Although swimming kinematics have been studied in detail for several species over many years, only a few studies have used a quantitative comparative approach and obtained high-resolution kinematic data from species such as tuna, which classically define one extreme of the fish swimming modes continuum (22, 23, 25).

Expected BCF kinematic patterns based on the classic swimming modes, such as a decreasing ratio of head:tail amplitude coupled with an increasing length of the propulsive wave from anguilliform to thunniform swimmers, were not observed in our comparative study. Instead, midline kinematics during steady swimming represent a continuum across different morphological characteristics, life stages, and native environments. Even when only selecting the four species that the traditional canonical classification is based on, we observed a significant overlap: most of the kinematic parameters were not significantly different across each category, and we even noted a kinematic pattern opposite to the classically expected one, with tuna having a significantly higher, rather than lower, head:tail oscillation amplitude (Fig. 1). Significant overlaps in BCF fish swimming kinematics may be the product of evolutionary constraints on fish propulsion resulting from hydrodynamic demands of moving through the dense and viscous aquatic medium. Head oscillation during swimming may be linked to locomotor efficiency by generating leading-edge suction and thus contributing to thrust (26). We expect fish with narrow tails and no caudal peduncle, such as eels, to have greater head and body amplitude. As their tail span is small with regards to their length, they are assumed to recruit more of their body to generate thrust (27). While this assumption may be valid, head oscillation may also be regulated in some species to enhance respiration and flow sensing (28). This may explain the pattern of species with stiffer bodies, such as those classified as carangiform and thunniform, to oscillate their head during swimming to an extent similar to other fish species and why a quantitative analysis of locomotor kinematics contradicts the long-held assumption that body stiffness and shape alone could inform swimming behavior.

The amplitude of the undulating wave along the body was also observed to be consistent across species, with median values ranging from 0.03 at the head to a maximum of 0.3 BL at the tail. This agrees with previous studies on a variety of species: dace *Leuciscus leuciscus* (29), trout (10), bluegill sunfish (30), goldfish *Carassius auratus* (29), eels (31), largemouth bass (32), saithe *Pollachius virens* (33), mackerel (33), and yellowfin tuna (34, 35) in which amplitude along the body increased in a rostro-caudal axis from 0 to 0.03 to a maximum of 0.2 to 0.3 BL. The amplitude envelope during BCF locomotion was well described by second-degree polynomial equations for 92% of the tested individuals. A unifying model, fitted using these individuals, was able to describe 60% of the variability in amplitude along the body across all tested species. The midlines that could not be correctly modeled with this equation belonged to species such as amphioxus, kingfish *Menticirrhus americanus*, flathead mullet *Mugil cephalus*, spadefish, rainbow trout, and largemouth bass, some of them being already identified as "noise" points in the multivariate clustering analysis. The coefficients of the equation covary, and their variance captures the diversity in BCF locomotion patterns (Fig. 3*C*). Engineers often base their robotic platforms on fish midline kinematics while deciding on segment formation (e.g., number of segments and position of joints) and control parameters (36). Polynomial coefficients presented in Fig. 3 provide a comprehensive picture of the

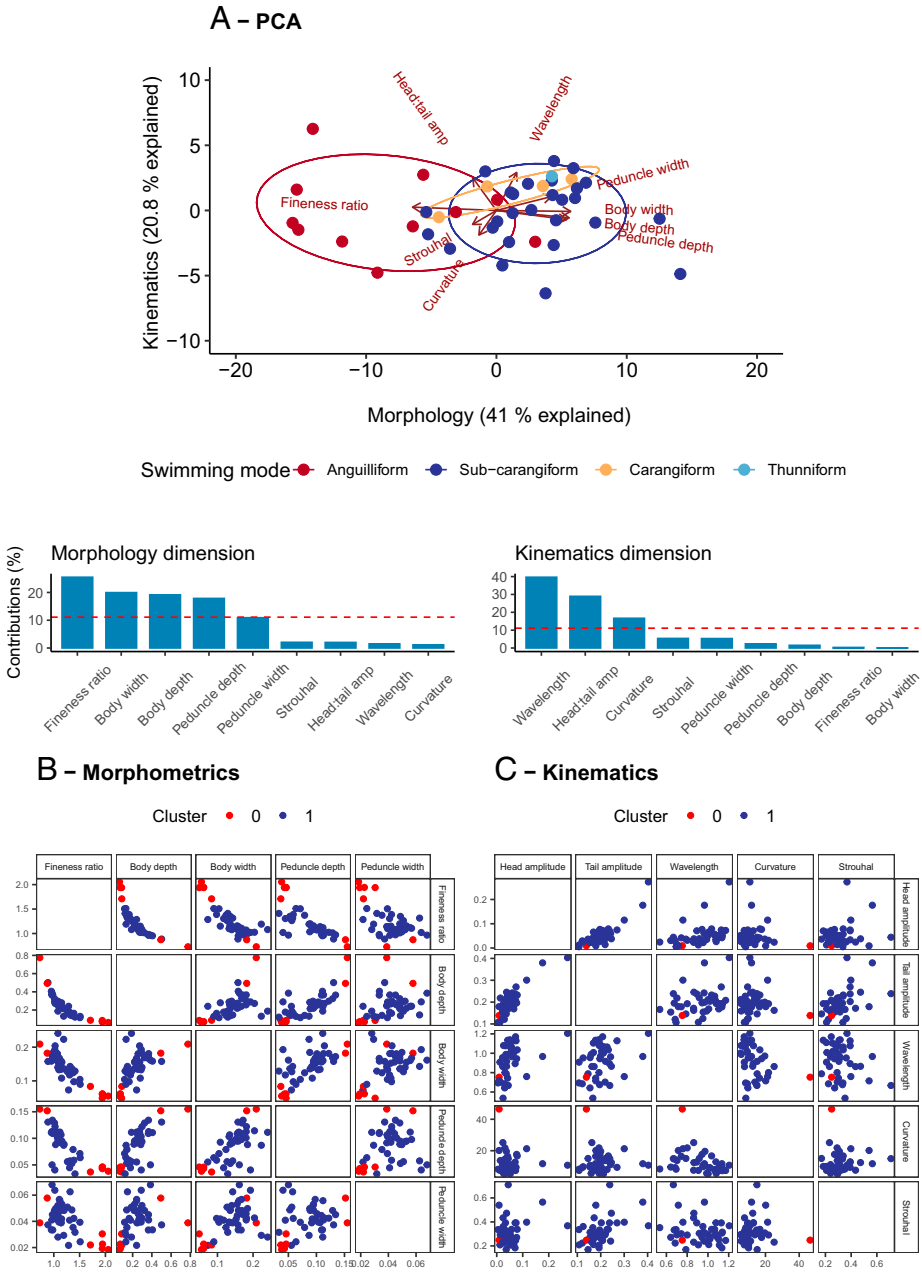

Fig. 4. Morphology is the principal axis of variation among species, not kinematics. (*A*) A PCA shows that most variation is expressed on the horizontal axis (first component; "morphology") with species classified as "anguilliform" being defined by a high body fineness ratio. The histograms show the relative contribution of each variable to the principal components retained with a red dashed line showing individual contributions below 10% as negligible for the component. (*B* and *C*) A density-based clustering analysis showing that analysis conducted on morphometric parameters identified one large cluster comprising most of the species (cluster 1; blue dots) and a few noise points consisting of species characterized by a high fineness ratio or a deeper body (cluster 0; red dots). The analysis conducted on kinematic parameters identified only one significant cluster (blue dots), meaning that all tested species exhibited a similar suite of two-dimensional midline kinematics.

biological design space and may correlate with high swimming efficiency and, hence, point to energetically efficient robotic designs.

Despite this broad similarity in amplitude patterns, we also observed both intra- and interspecific variability in body oscillation amplitude, especially in species traditionally classified as anguilliform swimmers. While eels and adult sea lampreys displayed amplitude patterns similar to those of salmonids, mackerel, and tuna, amphioxus and hagfishes exhibited a higher ratio of head to tail amplitude as well as higher values for amplitude along the body (Fig. 2 and *SI Appendix*, Figs. S6 and S7). There may be an evolutionary explanation for these differences. Amphioxus is a basal benthic chordate, and hagfishes are included in agnathan fishes, and both possess a continuous flexible notochord instead of a true backbone (37). Their ability to actively modulate body stiffness may thus be reduced compared to sharks or ray-finned species, which would explain their increased body oscillation amplitude. The sea lamprey, another jawless species which possesses a notochord, however, exhibits a median amplitude near 0.03 BL.

Previous studies (25) have also related the propulsive wavelength in swimming fishes to the number of vertebrae, suggesting

that a larger number of vertebrae or a continuous notochord would allow for an increased flexibility of the body and, hence, shorter propulsive wavelengths: body stiffness should be inversely proportional to wavelength. In the current study, the median length of the propulsive wave increased from anguilliform to thunniform swimmers, although not for all species. Species that would traditionally be classified in the anguilliform mode and expected to have a wavelength <1, such as amphioxus, showed a median wavelength of 1.14 BL. Atlantic salmon, which are expected to swim in the classical subcarangiform mode, exhibited a shorter median wavelength of 0.74 BL. Moreover, we observed high intra- and interspecific variability in wavelength, a pattern also shown by Long and Nipper (25). This variability suggests that the propulsive wave alone may not be a meaningful parameter to differentiate locomotor patterns among species and that intraspecific variability in swimming kinematics may be more substantial than previously appreciated. Curvature, or bending, along the body showed a consistent pattern across tested species, with a local minimum at ∼20 to 25% of body length and then increasing toward the tail. Species classified as anguilliform swimmers, however, showed higher variability as well as overall higher bending in the anterior part of their bodies. These species may exhibit a higher diversity in kinematics than species such as mackerel or tuna, which are more specialized for sustained higher-speed locomotion.

A combined multivariate analysis of morphometric and kinematic features did not identify groups of species with both similar morphology and kinematics, in contrast to a previous study that detected a correlation between body depth and locomotion style (23). One group of species characterized by a high fineness ratio of the body was identified (Fig. 4 *A* and *B*). However, these species did not exhibit a distinct suite of kinematics: some species in this group moved with greater amplitude (amphioxus and hagfishes) or shorter wavelength (eel and lamprey), but other kinematic parameters were statistically similar to those of other species in this region of the multivariate space. As a consequence, these species did not form a distinct group in the density-based clustering analysis (Fig. 4 *B* and *C*).

There are some limitations pertaining to our results. First, we classified each species into one of the four canonical modes based on common use in the existing literature, which involves some inherent subjectivity. Second, we focus on steady undulatory locomotion, which represents only a portion of the diversity inherent to fish locomotion: for example, we did not study paired-fin propulsion and unsteady behaviors such as maneuvering or acceleration. Nevertheless, the canonical swimming modes were initially proposed in the context of steady undulatory locomotion, which is important for pelagic and upriver migrations as well as for high-speed swimming through linear river systems and obstacles. Finally, we did not consider the specific shape and location of paired and median fins in our morphometric and kinematic analyses. The location and shape of the fins are challenging to describe accurately both in live and museum specimens. Instead, we choose to focus on building a diverse dataset in terms of species and swim speeds during BCF swimming and to analyze body deformations in a standardized and comparative manner.

Our comparative kinematic study of a wide diversity of fishes provides species-specific kinematic parameters (Dataset S2) and demonstrated that 1) there was no progressive trend in head:tail oscillation amplitude along the classical eel-to-tuna continuum; 2) body morphology rather than kinematic variables was the determining factor that produced grouping of fish species into the canonical swimming modes, suggesting that the classical separation of fish into swimming modes can in fact only accurately describe external body shape; 3) the propulsive wavelength increased from species classified as anguilliform to those classified as thunniform but with a large variability within and among species; 4) with the exception of tail beat frequency, two-dimensional kinematics during steady locomotion did not correlate significantly with swimming speed; and 5) BCF swimmers shared a broadly similar suite of two-dimensional kinematics during steady locomotion, with oscillation amplitude accurately modeled by a second-degree polynomial equation. Based on these results, we encourage biologists and engineers to rethink the use of the canonical categories of BCF locomotion in fishes, which can lead to bias in data interpretation and errors in computational studies that use incorrect kinematic data as inputs. An improved understanding of swimming kinematics also has relevance to conservation. For example, by applying the quadratic formula to model the amplitude envelope of target species, it is possible to identify size limits for slots and gaps in fishways and to design bycatch-reducing devices in fishing gear. While more work is needed to uncover the anatomical and hydrodynamic constraints and mechanisms underlying both the similarities and diversity in two-dimensional kinematics among species, we suggest that the explicit and widespread use of the four classic swimming modes is no longer appropriate.

Materials and Methods

Animals. Adult individuals (n = 1 to 6) from 43 species of fish and one species of basal chordate, the Mediterranean amphioxus, were filmed during steady swimming experiments at four different facilities: Harvard University (Institutional Animal Care and Use Committee, IACUC No. 20–03), the US Geological Survey (USGS) S. O. Conte Anadromous Fish Research Center (IACUC No. LB00TGC), the Whitney Laboratory at the University of Florida (IACUC No. 201603267), and the Greenfins Facility at the University of Rhode Island (IACUC No. 20–03). Most animals were of wild origin and were collected by nets, traps, or electrofishing.

Data Collection. Swimming experiments were performed using four different apparatuses: a 1 × 0.30 × 0.30 m flow tank at Harvard University, a recirculating flow tank respirometer (Loligo Systems, test section = 0.88 × 0.25 × 0.25 m, volume = 185 L) at the University of Florida, a circular tank (diameter = 12 m; volume = ∼475 m^3) at the University of Rhode Island's Greenfins tuna facility, and a 35 × 0.63 × 0.63 m experimental flume with a large staging area at the USGS S. O. Conte Anadromous Fish Research Center (*SI Appendix*, Fig. S1). Fish were tested under flow velocities ranging from 0 to 4.5 m × s^{-1}, resulting in a range of swimming speeds from 0.2 to 25 BL × s^{-1}. While the first three setups aimed at measuring sustained swimming ability, the USGS's experimental flume allowed us to measure volitional high-speed steady swimming as well as sprinting ability. This large flume was instrumented with 16 synchronous half-duplex Passive Integrated Tag (PIT) receivers recording the movements of fish tagged with 12- or 23-mm PIT tags (Texas Instrument Registration and Identification System instrument). This allowed for the unique identification of all fish tested in this apparatus. Ventral or dorsal views of the fish were recorded during steady swimming by high-speed video cameras (FASTCAM 1024 PCI, Photron; Hi-Spec1, Fastec Imaging; Phantom V1212) at 120 to 1,000 frames × s^{-1}. Tunas swimming at the Greenfins facility were filmed from above the tank at 120 frames × s^{-1} using a GoPro Hero 3. Frames from video sequences were calibrated using direct linear transformation (pixels to centimeters) in ImageJ (NIH). A sequence corresponding to one complete cycle of caudal fin movement was extracted for each individual. Starting at the tip of the nose and ending at the tip of the caudal fin, the midline of the fish was digitized at least 10 times within each tailbeat cycle in MATLAB (MathWorks) using custom code ("CurveMapper," *SI Appendix*). A spline curve was fitted to the points selected along the midline of the fish in order to generate 200 equally spaced x,y coordinates for each midline (0 = tip of snout and 200 = tip of tail).

Kinematic Analyses. All kinematics data extractions were performed using custom-written scripts in R and MATLAB. Midline x,y coordinates were imported into R (38) and standardized to BL. The ground speed was calculated based on the video recordings: the distance traversed by the tip of the tail between the first and the last midline was divided by the time elapsed during the movement. The swim speed was then calculated by adding the average free-stream velocity to the groundspeed. To ease visualization, each clip was rotated so that the mean direction of motion was parallel to the longitudinal plane (x-axis). To account for any forward movement made by fish swimming with a positive groundspeed, the most anterior point of each rotated midline

was translated such that it was fixed at location x = 0. These transformations had no effect on the inherent properties of the movement. Kinematic variables were calculated on the adjusted midline coordinates and expressed in units of BL. The tailbeat frequency was calculated by dividing the frame rate by the total number of frames in a single stride. Stride length was calculated by dividing the fish swim speed by the tailbeat frequency.

During steady swimming, each point along the body midline oscillates back and forth periodically. The amplitude of this undulatory movement was determined as the maximal excursion on the *y*-axis for each of the 200 locations along the body of the fish. Head and tail amplitude were defined as amplitude for locations 1 through 5 (head) and 195 through 200 (tail), respectively. The location of minimal and maximal amplitude and the ratio of head:-tail amplitude were also quantified. We measured the timing (phase) of these oscillations to evaluate how midline points move with respect to each other using a method described in Akanyeti and Liao (39). We used a second-order polynomial to model the fish amplitude envelopes (i.e., how peak-to-peak amplitude, y, varies along the body, x, over the course of a single tailbeat),

$$y = \beta_0 + \beta_1 x + \beta_2 x^2.$$

The coefficients of the polynomial (B_{0-3}) were estimated using the least-squares method, and the goodness of the fit was evaluated using the r-squared value. This model was estimated first for all individual fish datasets; those with $R^2 \geq 0.9$ were then used to estimate the global model.

Curvature, defined as the reciprocal of the radius of curvature ($K = 1 \times R^{-1}$) in two dimensions, was calculated across the tailbeat cycle for each location along the body of the fish using three points equally distant on a distance of 0.05 (5%) of the body length: the location itself, the fifth location anteriorly, and the fifth location posteriorly.

The speed and length of the propulsive wave were measured by identifying bending moments along the fish's body. The speed of the propulsive wave was measured by sequentially identifying the peak of the wave as it moved posteriorly along the body. Peaks were identified as locations of maximum displacement on the *y*-axis (*Y*) at location (*L*); Y_L was a local peak if

$$Y_{L-1} < Y_L > Y_{L+1},$$

in which Y_{L-1} is the lateral displacement at the next anterior location, and Y_{L+1} is the lateral displacement at the next posterior location. The first midline corresponds to the moment when the fish tail was at the top of its stride (i.e., the tip of the tail was at its location of greatest lateral excursion on the *y* axis). On each successive midline, the next posterior position of the peak was identified until the body returned to the top of its stride, and the peak of the wave passed the tip of the tail. The location of each wave peak was plotted against its associated midline number and evaluated for collinearity. Any deviation from collinearity ($R^2 < 0.9$) was considered potential evidence of error from image distortion and/or digitizing, and clips showing this potential error were further evaluated to ensure the accuracy of the position of the peak. The speed of the wave was then quantified by fitting a linear regression through the points following the standard formula

$$\hat{L} = a + bP_{TB},$$

in which $\hat{L}$ (the location of the wave peak along the body in BL) is described by an intercept (*a* in BL) and a slope (b in BL × tailbeat^{-1}) × P_{TB} (the proportion of a tailbeat covered in a single midline). The slope (*b*) represents the speed at which the wave passes down the body in a single tailbeat. As there can only be one tailbeat per wave, the slope is also the length of the propulsive wave (in BL). To express it in units of BL × s^{-1}, the wave speed was multiplied by tailbeat frequency.

Finally, Re was calculated on the basis of the swimming speed of the fish, its body length, and kinematic viscosity of 1 mm^2 × s^{-1}. The ST was calculated by multiplying tailbeat frequency by tail amplitude and then dividing the product by swim speed.

Morphological Measurements. Specimens (n = 1 to 3) from each species were obtained from the Fish Collection at the Harvard Museum of Natural History. Dorsal and lateral photographs of individuals of similar size as the ones used in the current study were taken to obtain linear measurements such as standard length (SL), fork length, body width, and body depth at 10, 25, 50, 75, 90, and 100% of SL, maximum body width, and depth as well as their position along the body. To standardize our measurements, we used the open-source FishMeasurements MATLAB code (https://gitlab.com/robintha/027-matlab-fish-measurements). All measurements were reported as a proportion of standard BL. A dimensionless number, the fineness ratio, was calculated by dividing the SL by the elliptical mean of body depth and width using an equation adapted for BCF swimmers (40).

Statistical Analysis. Descriptive statistics were computed for kinematic variables, and mean values were compared across species classified into the a priori swimming modes using a one-way ANOVA followed by a Tukey–Kramer multiple comparison test ($\alpha = 0.05$) with post hoc power analysis. A PCA was used to assess how the species tested in this study may cluster in the multivariate space of the measured kinematic and morphometric variables. The swimming speed and correlated variables such as tail beat frequency, stride length, and Re were excluded. The PCA included nine variables: head:tail amplitude, maximum curvature, ST, wavelength, fineness ratio, maximum peduncle depth, maximum peduncle width, maximum body depth, and maximum body width. These were averaged by species and centered prior to the PCA. Each species was then assigned a posteriori to one of the canonical swimming modes ("anguilliform," "subcarangiform," "carangiform," or "thunniform") based on experience and existing literature on fish locomotion. A nonparametric density-based clustering approach (41) was then used to identify natural groups among the studied species based on 1) morphometrics and 2) undulatory kinematics. Without assuming any a priori grouping of the data, the dbscan algorithm identifies areas of high density in the multidimensional data space and assigns data points to the same cluster if they are density reachable from each other (41). Unassigned points are considered noise. Clustering analyses for morphometric and kinematics data were done by using a minimum density of six points and a radius of 4.5 and 0.12, respectively. The optimal radius was found empirically by plotting the distribution of the Euclidian distances to nearest neighbors for all data points (KNN-dist). All analyses were performed in R version 3.6.2 or JMP (v. 15, SAS). One species with missing data for body length, the chain catshark *Scyliorhinus retifer*, was excluded from the multivariate analyses.

Data Availability. All data and code that support the findings of this study are available on Dryad (https://doi.org/10.5061/dryad.bg79cnp9x) (42). Original videos and photographs are available from the authors upon request.

ACKNOWLEDGMENTS. This research was supported by the Office of Naval Research Grants N000141410533 and N00014-15-1-2234 and NSF Grant 093088-17158 to G.V.L.; the Carl Tryggers Foundation Grant (20:98) to V.D.S.; Fonds de Recherche Nature et Technologies du Québec to E.G.; Great Lakes Fisheries Commission Grant 2017_CAS_54063 to E.G. and T.C.-S.; National Oceanic and Atmospheric Administration Fisheries Grant SER-2019-007 to T.C.-S.; the NSF Grants (IOS1257150 and IOS1856237), National Institute on Deafness and Other Communication Disorders Grant RO1-DC-010809, Anonymous Foundation Grant, Patagonia Conservation Grant, and University of Florida Research Opportunity Seed Grant to J.C.L.; the NSF Grant PRFB1907156 to D.K.W.; Cymru Cofund Fellowship (663830-AU167); and the European Commission Grants (H2020-MSCA-RISE-2019, 873178) to O.A. The work was supported by the staff of each research facility involved in the project, and we especially thank Peter Mottur and Prof. Terry Bradley for allowing access to the Greenfins Tuna Facility at the University of Rhode Island. We thank J. Lim for providing some of the videos used in this study, G. Andres for his help with data acquisition, R. Thandiackal for the design of the FishMeasurements code, and D. Irschick and P. Webb for their helpful comments on the manuscript. Any use of trade, product, or firm names is for descriptive purposes only and does not imply endorsement by the government of the United States.

1. J. Gray, How fishes swim. *Sci. Am.* **197**, 48–55 (1957).
2. S. Vogel, *Life in Moving Fluids: The Physical Biology of Flow-Revised and Expanded* (Princeton University Press, ed. 2, 2020).
3. V. Di Santo, C. P. Kenaley, G. V. Lauder, High postural costs and anaerobic metabolism during swimming support the hypothesis of a U-shaped metabolism-speed curve in fishes. *Proc. Natl. Acad. Sci. U.S.A.* **114**, 13048–13053 (2017).
4. V. Di Santo, C. P. Kenaley, Skating by: Low energetic costs of swimming in a batoid fish. *J. Exp. Biol.* **219**, 1804–1807 (2016).
5. G. V. Lauder, E. D. Tytell, Hydrodynamics of undulatory propulsion. *Fish Physiol.* **23**, 425–468 (2005).
6. R. Zhu *et al.*, "Computational study of fish-shaped panel with simultaneously heaving and bending motion" in *AIAA Scitech 2019 Forum, AIAA SciTech Forum* (American Institute of Aeronautics and Astronautics, 2019) https://doi.org/10.2514/6.2019-1655.
7. C. M. Breder, The locomotion of fishes. *Zoologica* **4**, 159–291 (1926).
8. C. Lindsey, "Form, function and locomotory habits in fish" in *Locomotion*, W. S. Hoar, D. J. Randall, Eds. (Elsevier, 1978), pp. 1–100.
9. J. Gray, Studies in animal locomotion: IV. The neuromuscular mechanism of swimming in the eel. *J. Exp. Biol.* **13**, 170–180 (1936).
10. R. Bainbridge, Caudal fin and body movement in the propulsion of some fish. *J. Exp. Biol.* **40**, 23–56 (1963).
11. P. W. Webb, Form and function in fish swimming. *Sci. Am.* **251**, 72–83 (1984).
12. A. J. Smits, Undulatory and oscillatory swimming. *J. Fluid Mech.* **874**, p. 1 (2019).

13. T. Watson, How giant marine reptiles terrorized the ancient seas. *Nature* **543**, 603–607 (2017).
14. R. Motani, H. You, C. McGowan, Eel-like swimming in the earliest ichthyosaurs. *Nature* **382**, 347–348 (1996).
15. U. K. Müller, J. L. Van Leeuwen, Undulatory fish swimming: From muscles to flow. *Fish Fish.* **7**, 84–103 (2006).
16. S. Fujiwara, S. Yamaguchi, Development of fishlike robot that imitates carangiform and subcarangiform swimming motions. *J. Aero Aqua Bio-mech.* **6**, 1–8 (2017).
17. M. Sfakiotakis, D. M. Lane, J. B. C. Davies, Review of fish swimming modes for aquatic locomotion. *IEEE J. Oceanic Eng.* **24**, 237–252 (1999).
18. N. Li, H. Liu, Y. Su, Numerical study on the hydrodynamics of thunniform bio-inspired swimming under self-propulsion. *PLoS One* **12**, e0174740 (2017).
19. T. Castro-Santos, A. Cotel, P. W. Webb, Fishway evaluations for better bioengineering - an integrative approach, in *Challenges for Diadromous Fishes in a Dynamic Global Environment*, A. J. Haro, *et al.*, Eds. (American Fisheries Society, Symposium 69, Bethesda, MD, 2009), pp. 557–575.
20. S.-J. Park *et al.*, Phototactic guidance of a tissue-engineered soft-robotic ray. *Science* **353**, 158–162 (2016).
21. G. V. Lauder, V. Di Santo, "Swimming mechanics and energetics of elasmobranch fishes" in *Fish Physiology*, R. E. Shadwick, A. P. Farrell, C. J. Brauner, Eds. (Academic Press, 2015), pp. 219–253.
22. J. Zhu *et al.*, Tuna robotics: A high-frequency experimental platform exploring the performance space of swimming fishes. *Sci. Robot.* **4**, eaax4615 (2019).
23. J. F. van Weerden, D. A. Reid, C. K. Hemelrijk, A meta-analysis of steady undulatory swimming. *Fish Fish.* **15**, 397–409 (2014).
24. L. Wen *et al.*, Understanding fish linear acceleration using an undulatory biorobotic model with soft fluidic elastomer actuated morphing median fins. *Soft Robot.* **5**, 375–388 (2018).
25. J. H. Long Jr., K. S. Nipper, The importance of body stiffness in undulatory propulsion. *Am. Zool.* **36**, 678–694 (1996).
26. K. N. Lucas, G. V. Lauder, E. D. Tytell, Airfoil-like mechanics generate thrust on the anterior body of swimming fishes. *Proc. Natl. Acad. Sci. U.S.A.* **117**, 10585–10592 (2020).
27. E. D. Tytell, G. V. Lauder, The hydrodynamics of eel swimming: I. Wake structure. *J. Exp. Biol.* **207**, 1825–1841 (2004).
28. O. Akanyeti *et al.*, Fish optimize sensing and respiration during undulatory swimming. *Nat. Commun.* **7**, 11044 (2016).
29. R. Bainbridge, The speed of swimming of fish as related to size and to the frequency and amplitude of the tail beat. *J. Exp. Biol.* **35**, 109–133 (1958).
30. O. Akanyeti *et al.*, Accelerating fishes increase propulsive efficiency by modulating vortex ring geometry. *Proc. Natl. Acad. Sci. U.S.A.* **114**, 13828–13833 (2017).
31. G. B. Gillis, Environmental effects on undulatory locomotion in the American eel *Anguilla rostrata*: kinematics in water and on land. *J. Exp. Biol.* **201**, 949–961 (1998).
32. B. C. Jayne, G. V. Lauder, Speed effects on midline kinematics during steady undulatory swimming of largemouth bass, *Micropterus salmoides*. *J. Exp. Biol.* **198**, 585–602 (1995).
33. J. J. Videler, F. Hess, Fast continuous swimming of two pelagic predators, saithe (*Pollachius virens*) and mackerel (*Scomber scombrus*): A kinematic analysis. *J. Exp. Biol.* **109**, 209–228 (1984).
34. H. Dewar, J. Graham, Studies of tropical tuna swimming performance in a large water tunnel - energetics. *J. Exp. Biol.* **192**, 13–31 (1994).
35. J. M. Donley, K. A. Dickson, Swimming kinematics of juvenile kawakawa tuna (*Euthynnus affinis*) and chub mackerel (*Scomber japonicus*). *J. Exp. Biol.* **203**, 3103–3116 (2000).
36. S. E. A. W. Fetherstonhaugh, Q. Shen, O. Akanyeti, Automatic segmentation of fish midlines for optimizing robot design. *Bioinspir. Biomim.* **16**, 046005 (2021).
37. K. S. Thomson, The adaptation and evolution of early fishes. *Q. Rev. Biol.* **46**, 139–166 (1971).
38. R Core Team, *R: A Language and Environment for Statistical Computing*. R Foundation for Statistical Computing, Vienna. https://www.r-project.org/ (Accessed 29 November 2021).
39. O. Akanyeti, J. C. Liao, A kinematic model of Kármán gaiting in rainbow trout. *J. Exp. Biol.* **216**, 4666–4677 (2013).
40. J. A. Walker, M. E. Alfaro, M. M. Noble, C. J. Fulton, Body fineness ratio as a predictor of maximum prolonged-swimming speed in coral reef fishes. *PLoS One* **8**, e75422 (2013).
41. M. Hahsler, M. Piekenbrock, D. Doran, dbscan: Fast density-based clustering with R. *J. Stat. Softw.* **91**, 1–30 (2019).
42. E. Goerig *et al.*, Convergence of undulatory swimming kinematics across a diversity of fishes. Dryad. https://doi.org/10.5061/dryad.bg79cnp9x. Deposited 4 November 2021.